EARTHQUAKE SPECTRA

The Professional Journal of the Earthquake Engineering Research Institute

PREPRINT

This preprint is a PDF of a manuscript that has been accepted for publication in *Earthquake Spectra*. It is the final version that was uploaded and approved by the author(s). While the paper has been through the usual rigorous peer review process for the Journal, it has not been copyedited, nor have the figures and tables been modified for final publication. Please also note that the paper may refer to online Appendices that are not yet available.

We have posted this preliminary version of the manuscript online in the interest of making the scientific findings available for distribution and citation as quickly as possible following acceptance. However, readers should be aware that the final, published version will look different from this version and may also have some differences in content.

The DOI for this manuscript and the correct format for citing the paper are given at the top of the online (html) abstract.

Once the final, published version of this paper is posted online, it will replace the preliminary version at the specified DOI.

Development of Fragility Curves for Confined Masonry Buildings in Lima, Peru

Holger Lovon,[a] Nicola Tarque[a], Vitor Silva,[b] and Catalina Yepes-Estrada[b]

This paper aims at investigating the seismic fragility of confined masonry structures in Lima (Peru), which can be used to perform earthquake scenarios at urban scale. A database describing the geometric properties (walls density, building area, height) of this type of structures was developed using data from field surveys. This information was complemented with results from experimental tests to compute a large set of capacity curves using a mechanical procedure. These models were tested against a set of ground motion records using the displacement-based earthquake loss assessment (DBELA) procedure, and the structural responses were used to derive fragility functions for four building classes. The resulting fragility curves were convoluted with seismic hazard curves to evaluate the annualized expected loss ratio and annual collapse probability.

INTRODUCTION

Confined masonry (CM) has been one of the most common types of construction in the Peruvian coast. In the capital Lima, with a population of almost 10 million people, confined masonry buildings represent about 56% of the total building stock (Yepes-Estrada *et al.*, 2017). The majority of these structures are built without following adequate construction practices (i.e. without the consideration of modern seismic codes), mostly due to the low risk awareness of the inhabitants and an inefficient legal enforcement. According to Blondet *et al.* (2004), this trend in the informal construction is associated with Lima's rapid population growth, especially in the sub-urban areas. Given the expected poor seismic performance of informally built structures (Blondet *et al.*, 2004), their popularity, and the high seismic hazard in the region (e.g. Monroy & Bolaños, 2004), it is fundamental to understand their seismic fragility, and explore strategies to reduce their seismic risk.

[a] Pontificia Universidad Católica del Perú, 1801 Universitaria Ave., Lima, Perú
[b] GEM Foundation, Via Ferrata 1, Pavia, Italy

The 2007 M7.9 Pisco earthquake caused the collapse of around 76 000 buildings, where the majority of these structures were composed by adobe. However, according to the reconnaissance report by the Earthquake Engineering Research Institute (EERI, 2007), some of the confined masonry buildings with vertical (e.g. soft-story) or horizontal irregularities and/or bad detailing, collapsed or were heavily damaged. This finding was also corroborated by the damage observations from other earthquakes in Latin America, as reported by Rodriguez & Blondet (2004). The latter study evaluated losses and damage from the 2003 M7.6 Colima (Mexico), 1999 M6.2 Armenia (Colombia), and 1985 M7.8 Algarrobo (Chile) earthquakes.

Fragility functions establish the probability of exceeding a number of damage states conditional on a given ground shaking level. One of the first studies regarding fragility functions in Peru is presented by Kuroiwa *et al.* (2002), who processed earthquake damage in confined masonry buildings due to the 1996 M7.4 Chimbote earthquake to validate the fragility functions developed within the SISRA project (1985). Garcia and Degrande (2017) developed fragility functions for typical CM houses in Cuenca-Ecuador. The GAR-13 report (ONU, 2013) also presents fragility functions for CM buildings from 1 to 3 stories.

Most of the existing functions for Peru were defined in terms of macroseismic intensity (e.g. MMI), which can be used for rapid damage assessment using data from the *ShakeMap* system (Worden and Wald 2016). However, MMI-based functions cannot be directly used with modern ground motion prediction equations (GMPEs) whose results are usually expressed in terms of peak ground motion (acceleration or velocity) or spectral acceleration at a particular period of vibration (see Douglas and Edwards (2016) for a review of existing GMPEs). These functions are fundamental for the assessment of earthquake losses considering probabilistic seismic hazard (e.g. Yepes-Estrada and Silva 2017).

This paper investigates the seismic fragility of CM buildings (formal and informal) found in the Metropolitan Area of Lima with 1-story and 2-story, and employs the results to estimate two risk metrics: annual average loss ratios and annual collapse probabilities. For this purpose, field surveys from 120 buildings collected by Tarque and Mosqueira (2005) were used to develop a database with the most relevant structural characteristics for this type of construction. These datasets were used to fit statistical distributions to characterize each parameter, which were then employed to generate a large number of structural models representing a specific building class. The drift capacity was estimated using experimental

results from six tests performed at the Pontifical Catholic University of Peru (PUCP). The simplified procedure to evaluate the seismic capacity proposed by Restrepo-Velez (2004) and Borzi et al. (2008) was employed.

The seismic demand was represented by a set of ground motion records selected for the coast of Peru, considering the associated seismicity and tectonic environment (Garcia *et al*., 2017). Each structural model was tested against the set of ground motion records using the Displacement-based Earthquake Loss Assessment (DBELA) methodology (Crowley *et al*., 2004, Silva *et al.*, 2013), a simplified methodology which allows the consideration of the building-to-building and record-to-record variability, while maintain a low computational effort. This method compares the displacement capacity and demand at specific limit states in order to allocate the structures into a set of damage states. The resulting fragility functions were used to calculate the average annual loss ratio and collapse probability in Lima, using the probabilistic seismic hazard analysis (PSHA) model recently develop within the South America Risk Assessment (SARA) project (GEM, 2015).

CONFINED MASONRY BUILDINGS IN LIMA

CM buildings constructed in Lima share similar characteristics with those constructed in the coastal cities of Peru. In this work, both formal and informal CM buildings with 1 and 2 stories were considered. Typical CM buildings in Lima are shown in Figure 1.

Figure 1. Typical CM buildings in Lima.

INFORMAL CONFINED MASONRY BUILDINGS

This typology includes all buildings which were built without professional council. In order to characterize the informal CM buildings in Lima, a database was created based on building surveys carried out by Tarque and Mosqueira (2005). The inspections took place in Lima's districts with high concentration of CM buildings (e.g. Villa el Salvador, Carabayllo,

San Martin de Porres, Chorrillos, Ate, Puente Piedra and La Molina). The data cover relevant information concerning the number of stories, construction age, wall's dimensions, confinement dimensions, inter-story system, blueprints of wall distribution (see Figure 2), amongst others. For this study, 120 surveys were used to develop the database. The surveys include 1-story and 2-story informal CM buildings

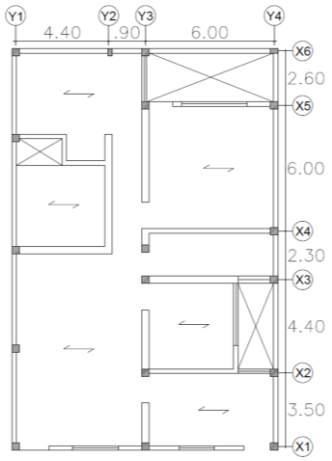

Figure 2. Typical plan view of a CM informal buildings, the X-axis is oriented in the parallel direction to the street, and the Y-axis is oriented in the perpendicular direction to the street.

Some of these buildings can present structural problems such as short columns, large openings, and horizontal and vertical irregularities. The majority of the walls in these buildings are constructed with non-solid partially industrialized bricks. Clay units cover up to 50% of the total area. Rope rigging arrangement is mostly used in the construction of the CM walls. The width of these elements varies between 150 and 250 mm (see Figure 3), and a lightened concrete slab of 200 mm thick usually composes the roof or floor area. The roof can also be composed by zinc sheets or wooden planks, depending on the economic resources of the householder. Buildings which present a high density of walls in one direction, and relatively short density in the other direction are very common (see Figure 2). Most of these buildings present horizontal and vertical irregularities (large openings) in their structural configuration. Structural walls present strip footing. The reinforcement of the columns is usually composed by four 12.7 mm longitudinal steel bars and ties spaced each 200 mm. These walls do not have horizontal reinforcement. The field surveys indicate that an important percentage of these buildings are built in stages (i.e. incremental construction).

A statistical treatment of the data was performed for variables related to the structural provisions, following the procedure described by Silva et al. (2014a). Goodness-of-fit tests were carried out on theses variables in order to fit appropriate probability distributions. The

chosen probability model and associated statistical parameters are presented in Table 1 and Table 2. It is also relevant to note that during the review of the building surveys, masonry walls with a high percentage of openings (usually to accommodate doors and windows) were found. Due to the inherent strength reduction, these elements were considered as "partially confined" walls. The diagonal compression resistance of CM walls was defined according to Tarque and Mosqueira (2005).

Table 1. Random variables for 1-story informal buildings

Variable	Description	Units	Mean	Standard deviation	Statistical distribution
A_T	Building area	m^2	96.8	43.0	Normal
h	Height	M	2.58	0.12	Normal
τ	Diagonal compression resistance	MPa	0.60	0.12	Normal
ρ_d	Confined walls density x-x	%	1.32	1.11	Lognormal
	Confined walls density y-y	%	4.84	1.83	Lognormal
	Partially confined walls density x-x	%	3.02	1.54	Lognormal
	Partially confined walls density y-y	%	1.20	1.05	Lognormal
n_c	Confinement columns density x-x	$\#/m^2$	0.13	0.04	Lognormal
	Confinement columns density y-y	$\#/m^2$	0.15	0.04	Lognormal

Table 2. Random variables for 2-story informal buildings

Variable	Description	Units	Mean	Standard deviation	Statistical distribution
A_T	Building area	m^2	104.9	32.9	Normal
h	Height	m	2.57	0.12	Normal
τ	Diagonal compression resistance	MPa	0.60	0.12	Normal
ρ_d	Confined walls density x-x	%	1.51	0.99	Lognormal
	Confined walls density y-y	%	5.32	2.41	Lognormal
	Partially confined walls density x-x	%	2.1	1.50	Lognormal
	Partially confined walls density y-y	%	1.04	0.50	Lognormal
n_c	Confinement columns density x-x	$\#/m^2$	0.13	0.04	Lognormal
	Confinement columns density y-y	$\#/m^2$	0.14	0.04	Lognormal

FORMAL CONFINED MASONRY BUILDINGS

Formal confined masonry is built considering seismic provisions and with the involvement of structural engineers. These buildings usually do not have the structural problems presented for the informal counterpart. Clay units cover up to 30% of the total area, the width of the walls varies between 150 and 250 mm, a lightened concrete slab of 200 mm thick usually composes the roof or floor area, and structural walls have a strip footing. The confinement of the columns is similar to what was described for the informal buildings, but a horizontal steel reinforcement is usually applied.

In order to evaluate fragility curves for formal CM buildings, some of the previously presented parameters in Table 1 and Table 2 have to be adjusted according to the Peruvian seismic design code (NTP E.070). In particular, a minimum threshold for the wall density must be imposed according to Eq. (1).

$$\rho \geq \frac{ZUSN}{56} \quad (1)$$

where Z is a factor related to the seismic zone (i.e. 0.45g for Lima), U is a factor related to the use of the building (i.e. 1.0 for housing); S is a factor related to the soil (i.e. 1.05 for intermediate soil), and N is the number of stories.

The diagonal compression resistance is another important parameter that differentiates formal from informal construction. This parameter was defined according to the results of experimental tests on masonry walls (Manchego *et al*., 2016). A normal probability density function with a mean of 1.25 MPa and a standard deviation of 0.2 was assumed. The last parameters affecting the performance of informal and formal construction are the yielding and ultimate drifts, as described in the following section. Additional information about confined masonry in Peru can be found in the World Housing Encyclopedia reports by Loayza and Blondet (2002a, 2002b).

DERIVATION OF THE DRIFT CAPACITY USING EXPERIMENTAL TESTS

The results from two experimental campaigns using static in-plane tests were used to estimate the drift capacity of confined masonry walls, which are then used in the following section to calculate the displacement capacity. Both these campaigns were carried out at the PUCP structural laboratory, as described in Manchego *et al*. (2016) for the formal construction, and in Araoz and Velezmoro (2012) and Salinas and Lázares (2007) for the informally built structures. This section briefly summarizes the testing procedure, as well as the resulting drifts.

The geometric characteristics of the walls and the reinforcement ratio of the confined elements considered by Manchego *et al*. (2016) were representative of a typical formally built confined masonry structure in Lima. Clay masonry units used in all tests were the ones available in Lima's market. These units are called "King Kong – 18 huecos" and they have 18 vertical holes in their surface (see Figure 3). The holes represent almost 50% of the total volume of the masonry units, and the dimensions of the bricks are 30x130x230 mm^3. The

mean compression resistance of the units was estimated in 12 MPa with a standard deviation of 1.3 MPa. The mortar had a proportion of 1:4 (cement:sand), and a compression strength of approximately 18 MPa with a standard deviation of 3.7 MPa. Prior to the cyclic tests, some additional tests were carried out to evaluate a number of material properties: compression strength, elasticity modulus, diagonal compression strength and shear modulus. These results are summarized in Table 3.

Table 3. Summary of previous experimental tests to characterize CM panels.

Material property	Mean (MPa)	Standard deviation (MPa)
Compression strength	9.50	0.70
Elasticity modulus	5700	705
Diagonal compression strength	1.25	0.14
Shear modulus	1920	350

Six walls were subjected to in-plane cyclic loading according to the FEMA 461 (2007) procedure. Dimensions, reinforcement and cyclic horizontal load history were the same for all the tests. Three of the walls were tested without axial load (NAL), whilst the other three walls were tested with axial load (WAL). For the WAL walls, a vertically distributed load of 175kN was applied along the top horizontal confinement element to simulate the typical gravity load in a 2-story building. The walls were constructed according to the local construction practices (e.g. percentage of brick holes, wall dimensions, lateral reinforcement in panels, confinement dimensions, and confinement, type of reinforcement). The experimental set up is presented in Figure 3.

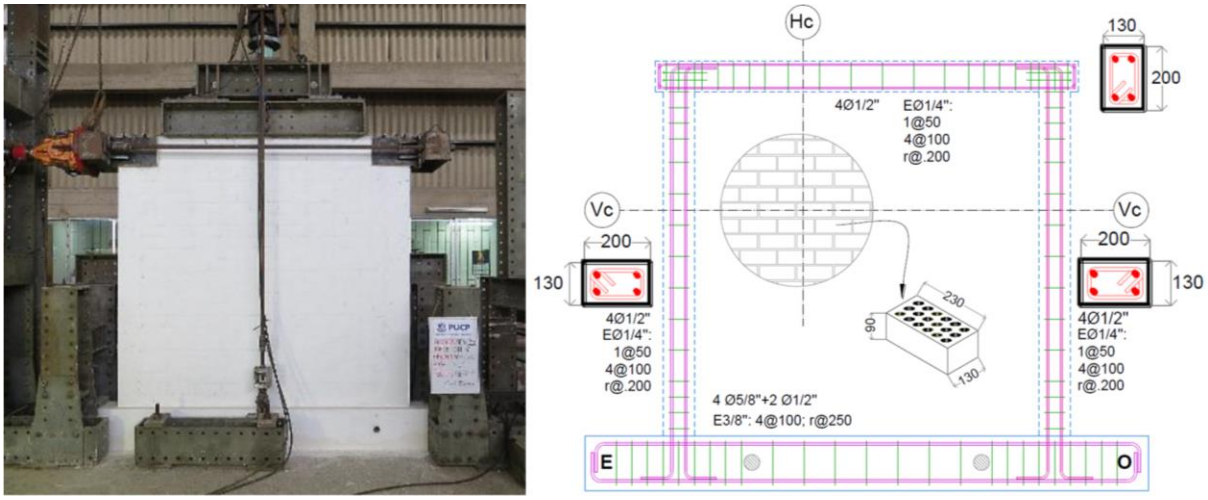

Figure 3. CM wall previous to the cyclic test (left). Construction details of CM walls (right).

The displacement-controlled history applied on all the CM walls was defined according to FEMA 461 (2007). The results from the cyclic loading test on masonry walls are useful in order to identify key aspects (e.g. base shear capacity, lateral displacement capacity, hysteresis behavior), which can be used in the calibration of numerical models. The displacement at the center of the top beam was monitored during each test, along with the applied load. By plotting these variables for each wall, the envelop of the hysteretic behavior of the CM walls with and without the axial load was obtained (see Manchego *et al.*, 2016), as presented in Figure 4 and Figure 5, respectively. The Riahi et al. (2009) model was plotted in the push and pull experimental curves to verify the fitting in both cases.

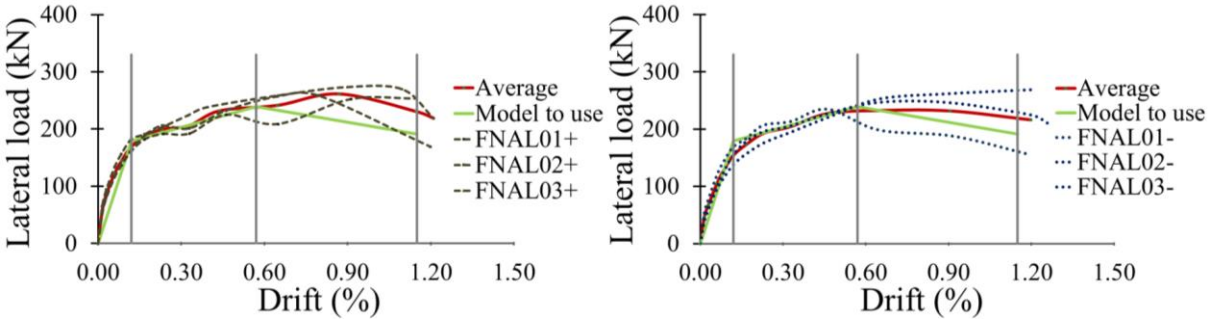

Figure 4. Capacity curves obtained from cyclic test of formal CM walls without axial load (FNAL). Left side for push (+), and right side for pull (-). Mean capacity curve (in red). Trilinear model adapted from Riahi et al. (2009) and Flores et al. (2001). Drifts for each control point (in brown) were defined based on the experimental curves.

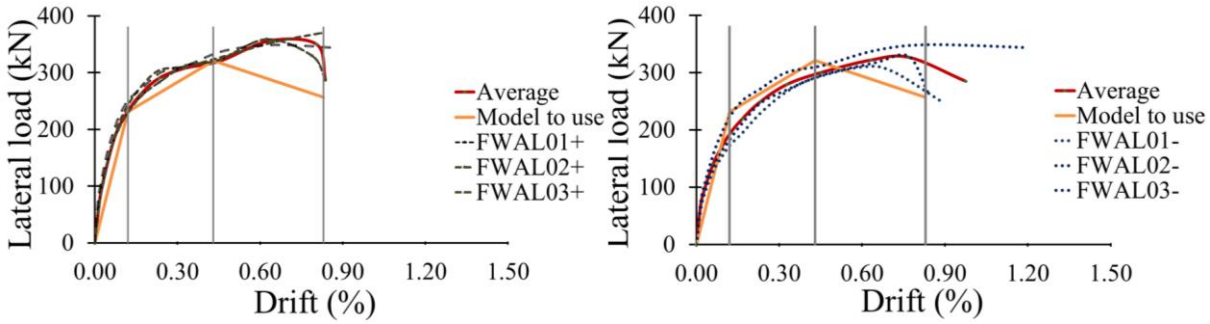

Figure 5. Capacity curves obtained from cyclic test of formal CM walls with axial load (FWAL). Left side for push (+), and right side for pull (-). Mean capacity curve (in red). Trilineal model adapted from Riahi et al. (2009) and Flores et al. (2001). Drifts for each control point (in brown) were defined based on the experimental curves.

As previously mentioned, for the informal CM buildings a similar experimental campaign had been performed previously, as described in Araoz and Velezmoro (2012), Salinas and Lázares (2008) and San Bartolomé (2004). The results from these tests are presented in Figure 6 and Figure 7.

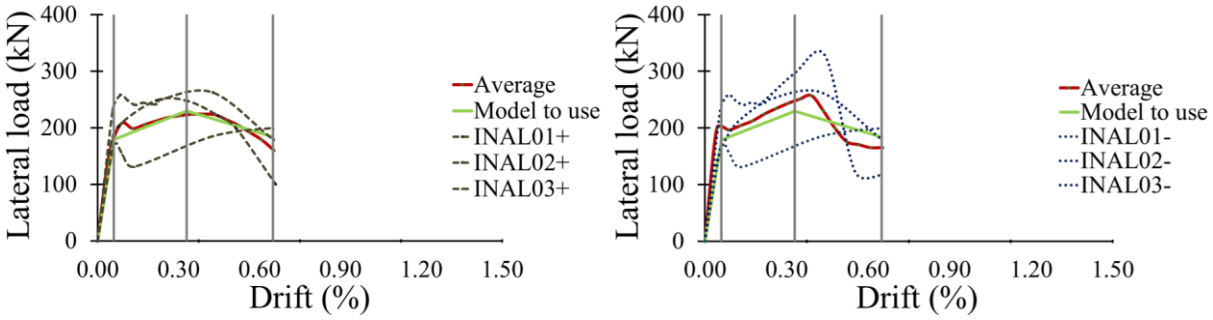

Figure 6. Capacity curves obtained from cyclic test of informal CM walls without axial load (INAL) adapted from Araoz and Velezmoro (2012), Salinas and Lázares (2008) and San Bartolomé. Left side for push (+), and right side for pull (-). Mean capacity curve (in red). Trilineal model adapted from Riahi et al. (2009) and Flores et al. (2001). Drifts for each control point (in brown) were defined based on the experimental curves.

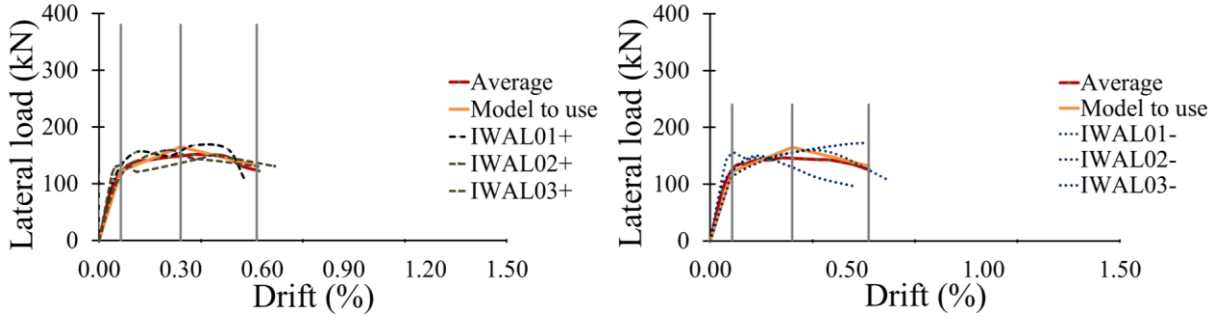

Figure 7. Capacity curves obtained from cyclic test of informal CM walls with axial load (IWAL) extracted from Araoz and Velezmoro (2012), Salinas and Lázares (2008) and San Bartolomé. Left side for push (+), and right side for pull (-). Mean capacity curve (in red). Trilineal model adapted from Riahi et al. (2009) and Flores et al. (2001). Drifts for each control point (in brown) were defined based on the experimental curves.

Several authors have studied the lateral resistance of confined masonry walls (e.g. Tomaževič and Klemenc (1997), Flores et al. (2001), Riahi et al (2009)). The vast majority of these studies agreed in the definition of an analytical capacity curve through 3 control points, as illustrated in Figure 8.

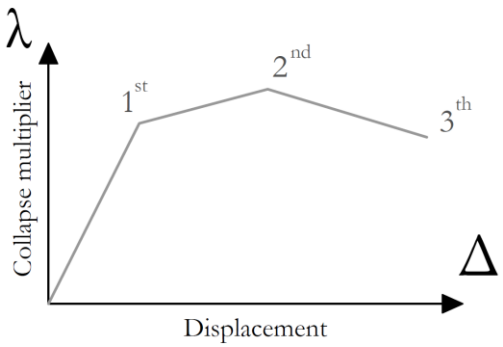

Figure 8. Control points defining the lateral resistance force of CM walls. Number 1 corresponds to the cracking; number 2 to the maximum shear force; and number 3 to the ultimate lateral force.

For the study presented herein, the Riahi et al (2009) and Flores et al. (2001) analytical expressions were slightly modified according to the experimental tests for the calculation of

the analytical capacity curve. The first control point was calculated according to the cracking shear resistance proposed by Riahi et al. (2009). The second control point was modified according to the confinement contribution proposed in Flores et al. (2001). The third control point was defined according to the ultimate resistance recommended in Tomaževič et al. (1997). Furthermore, 3 drift control points (i.e. yielding point, maximum base shear capacity, ultimate displacement) were identified in the experimental capacity curves based on the cracking process and cracking pattern. It is recognized that the greater the axial load, the more brittle is the behavior of the walls. This is the reason why the drift control points for walls with and without axial load were analyzed separately. The average drifts for the formal and informal CM walls are described in Table 4 and Table 5, respectively.

Table 4. Average drifts for each control point in formal CM walls obtained from experimental tests.

Control point	Drift NAL %	Drift WAL %
1	0.12	0.12
2	0.57	0.43
3	1.15	0.83

Table 5. Average drifts for each control point in informal CM walls according to Araoz and Velezmoro (2012), Salinas and Lázares (2007), and San Bartolomé (2004).

Control point	Drift NAL %	Drift WAL %
1	0.06	0.08
2	0.33	0.30
3	0.65	0.58

GENERATION OF CAPACITY CURVES

This section describes the methodology for the derivation of the capacity curves, which is strongly based on the recommendations by Restrepo-Velez (2004) and Borzi *et al*., (2008). Each capacity curve is represented by three pairs of collapse multipliers and displacements capacity. The former parameter is calculated using mechanics theory and the data from the building surveys, whilst the latter is computed using the experimental results described in the previous section. It is worth noting that buildings in Peru are often built adjacent to other structures, which may improve their seismic performance (i.e. higher capacity to dissipate energy), or increase significantly the seismic vulnerability (i.e. damage due to “pounding” effects or caused by different modes of vibration between adjacent structures due to distinct heights or stiffness). These effects were not explicitly accounted in this study.

CALCULATION OF THE COLLAPSE MULTIPLIER

A collapse mechanism is the sequence of processes that leads to the failure of the structure. Tomaževič and Gams (2012) tested scaled buildings of confined masonry and their experimental results show that damage in CM buildings is usually concentrated at the ground story, and less frequently at the upper floors, as illustrated in Figure 9. Similar findings were also presented by Calvi (1999) and Alcocer *et al.*, (2004). These failure mechanisms indicate that the inelastic behavior occurs mostly in a single story, and the structural behavior assumes that the building has rigid floor and roof diaphragms.

Out-of-plane failure mechanisms can also occur in masonry structures, but it is less frequent in CM buildings due to the confinement provided by the concrete and columns piers. Nonetheless, such failure can be considered using the procedures proposed by Doherty et al. (2002), Borzi et al. (2008) and Varela-Rivera et al. (2012). The latter study performed out-of-plane cyclic tests specifically on confined masonry walls.

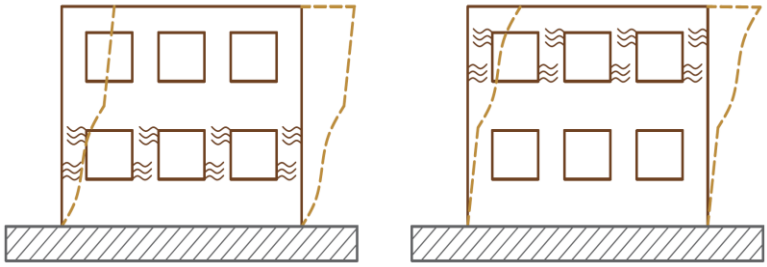

Figure 9. Collapse mechanism in CM buildings known as concentrated damage or soft story mechanism. Concentrated damage in the first floor (left), second floor (right) (adapted from Borzi et al. 2008).

The collapse multiplier represents the relationship between the lateral force and the weight of the building. Lateral resistance of CM buildings is given mainly by the walls density and resistance, and it can be withstood by a combination of flexure, shear and rocking mechanisms (e.g. Calvi 1999). Bennedeti and Petrini (1984) suggested a formulation to calculate the collapse multiplier in unreinforced masonry structures. According to this formulation, the collapse multiplier should be calculated for each story and each direction, and the lower collapse multiplier represents the global behavior of the structure. Borzi *et al.*, (2008) proposed a similar procedure for the calculation of this parameter. In the study presented herein, the Bennedeti and Petrini (1984) formulation was modified by changing its resistance model for the one defined in the previous section for CM walls (i.e. Riahi et al.,

2009; Flores et al., 2001). As a result, the following equations are proposed to calculate the collapse multiplier (1st, 2nd and 3rd point) for each floor and each direction:

$$\lambda_{i-d-1} = \frac{1}{W_T \frac{\sum_{k=i}^{n} h_k W_k}{\sum_{j=1}^{n} h_j W_j}} A_{i-d} \left[0.424\tau + 0.374 * \frac{\sum_{k=1}^{n} W_k}{A_i * (1+\gamma_{AB})} \right] \quad (2)$$

and

$$\lambda_{i-d-2} = \lambda_{i-d-1} + \frac{1}{W_T \frac{\sum_{k=i}^{n} h_k W_k}{\sum_{j=1}^{n} h_j W_j}} * \frac{1}{793.65} * \beta * n_{i-d} * \left[d_b^2 * \sqrt{f_c' * f_y} \right] \quad (3)$$

and

$$\lambda_{i-d-3} = 0.8 * \lambda_{i-d-2} \quad (4)$$

where $\lambda_{i-d-n}$is the collapse multiplier in the d-direction in the i-story for the n-control point (1, 2 or 3), W_T is the total weight of the building (kN), W_i is the weight of the i-story calculated as the weight per unit area and the total area of the building, h_i is the height of a i-story (m), A_{i-d} is the total shear wall area in the i-story in the d-direction (in m^2), τ is the diagonal compression resistance of the masonry (MPa), γ_{AB} is the ratio between A_{i-d} and B_{i-d} with B_{i-d} being the maximum area between the area of shear walls in the loaded direction and in the orthogonal direction, β is the efficiency factor related to the confinement columns (proposed as 0.3), n_{i-d} is the total number of columns in the loaded direction in the i-story, d_b is the diameter of the reinforcement bars, f_c' is the compression resistance of the concrete (MPa), and f_y is the yielding stress of the reinforcement steel (MPa).

For the calculation of the final shear area A_{i-d}, only 45% of the total area of the partially confined walls was considered. This reduction factor was proposed by Yañez et al. (2004), after the comparison of the shear capacity of walls with large openings under cyclic loading tests. Confinement columns located in the second floor and not constructed in the same axis as the first story were not considered.

Using the probabilistic distributions defined from the surveyed buildings, a random population of buildings per typology were generated, and used to calculate the aforementioned parameters, as presented in Figure 11.

CALCULATION OF THE DISPLACEMENT CAPACITY

Each building can be represented by a single-degree-of-freedom (SDOF) system, equivalent to the multi-degree-of-freedom (MDOF) counterpart in terms of mass, stiffness

and displacement capacity. According to the collapse mechanism described in the previous section, the deformed shape shown in Figure 10 illustrates the deformation of the structure in the linear and non-linear range. The linear shape can describe well the behavior of the structure along its height. The displacement capacity of the SDOF at the elastic limit point can be calculated by the following equation:

$$\Delta_y = k_1 h_T \delta_y \tag{5}$$

where h_T in the total height of the MDOF system, k_1 is the relationship between the total height of the MDOF and the height of the SDOF system in the elastic range, and δ_y is the maximum drift for the elastic behavior

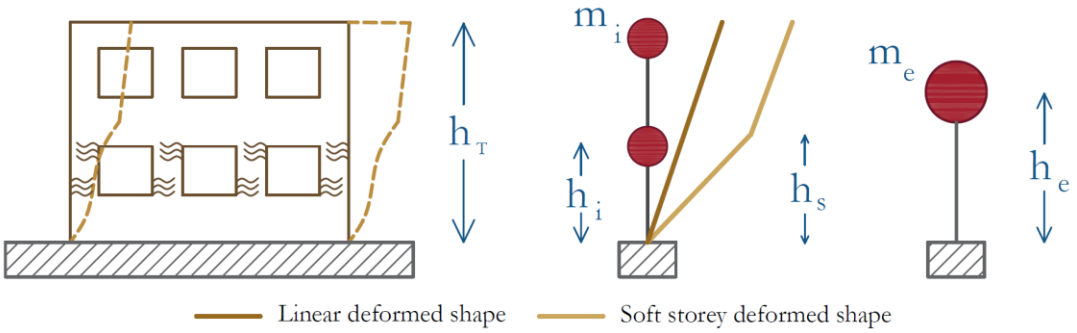

Figure 10. Deformation shape according to the collapse mechanism for the MDOF that represent the structure's behavior and its equivalent SDOF. m_i is the mass at i-story, h_i is the height at i-story, m_e is the equivalent mass and h_e is the equivalent eight of the SDOF, adapted from Borzi et al. (2008).

The deformation of the building in the nonlinear range can be represented by the elastic deformation plus the non-linear deformation of the weakest story, as expressed in the following equation:

$$\Delta_i = k_1 h_T \delta_y + k_2 (\delta_{CPn} - \delta_y) h_s \tag{6}$$

where k_2 is the relationship between the total height of the MDOF and the height of the SDOF system in the inelastic behavior; h_s is the height of the weakest story (defined as the story that has the lowest collapse multiplier), and δ_{CPn} is the drift values for the n-control point. The drift values were defined based on the previously presented experimental results (see Table 4 and Table 5). Restrepo-Velez (2004) proposed values for k_1 and k_2 as described in Table 6. These values were calculated by analyzing a simplified dynamic model which consisted in a distributed mass representing the masonry walls, and lumped masses representing each floor. The effective displacement is calculated for a given story at failure and for different levels of ductility.

Table 6. Values for k_1 and k_2 according to the number of floors

Number of Floors	k_1	k_2
1	0.79	0.96
2	0.71	0.95

Using Monte Carlo simulations, a random population of 100 buildings per class was generated according to the formulae and parameters proposed in Eq. 1 to Eq.6 and Table 1 to Table 6, as presented in Figure 11. The variables for 2-story buildings were generated per floor. Although Figure 11 shows a sample of 100 buildings per typology, the calculation of the fragility curves was carried out with 1000 capacity curves per typology to ensure convergence in the structural capacity (e.g. Silva et al. 2014b).

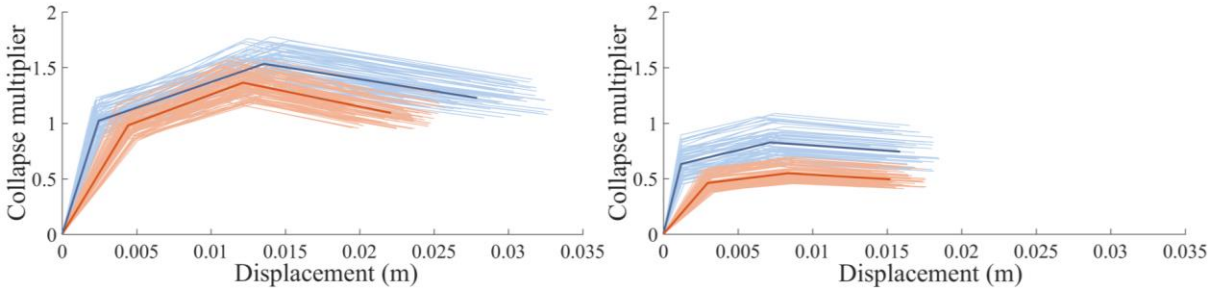

Figure 11. Sample of 100 building per typology: 1-story (blue) and 2-story building (orange), in terms of collapse multiplier and displacement capacity. Left side shows formal buildings capacity curve, and right side shows informal buildings capacity curve.

DEFINITION OF DAMAGE CRITERION

The damage states were defined according to the proposal by Lagomarsino and Giovinazzi (2006), who suggested limit states as a function of the notable points of the capacity curves. This damage criterion was corroborated by the cyclic tests described in previous sections as shown in Fig. 4 to Fig. 7. In this way, it is possible to consider the correlation between the structural capacity of the building and the expected damage thresholds.

Owing to the fact that masonry presents inelastic behavior for little displacements, slight damage occurs before the theoretical elastic displacement (Δ_1). In a similar manner, the moderate damage state is represented by the extension of the damages presented in the slight damage before the limit for the reparability is reached. Extensive damage is assumed to occur when the displacement for the maximum base shear is achieved (Δ_2). Finally, complete damage is defined at the last control point (Δ_3). The thresholds for each damage state as a

function of the notable points of the capacity curve is shown in Table 7, and illustrated in Figure 12.

Table 7. Damage threshold associated to Damage States.

Damage State	Damage Threshold
Slight	$0.7\ \Delta_1$
Moderate	$1.5\ \Delta_1$
Extensive	Δ_2
Collapse	Δ_3

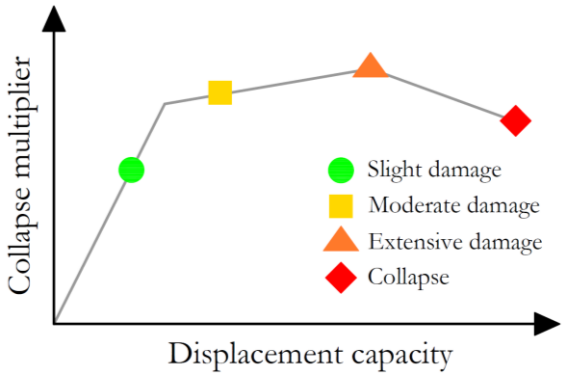

Figure 12. Representation of the damage states thresholds in the capacity curve.

CALCULATION OF THE SEISMIC DEMAND

The seismic demand is known to be one of the main sources of uncertainty in the development of fragility functions (Shome and Cornell 1999). Unlike the common belief that fragility is only structure-dependent, recent literature (e.g. Kohrangi *et al.*, 2017) has demonstrated that specific characteristics (e.g. duration, frequency content) of ground motion records can also influence significantly the resulting fragility functions. In this study, the selection of the ground motion records was performed considering the tectonic environment and seismicity in the coast of Peru. The seismic activity is mostly caused by the subduction process between Nazca and South American plate (Tavera and Buforn 2001). This deformation causes frequent and often large interplate earthquakes at depths between 10 km to 60 km, as well as shallower events of moderate magnitude. For long distances ($R > 50$ km), ground motion records with moment magnitudes between 7 and 9 were selected, while for shorter distances ($R \leq 50$ km), records with moment magnitudes between 5 and 7 were considered. Events recorded at less than 15 km were not considered in order to avoid near-fault effects, and only rock soil records were considered. Following this selection criterion, a set of ground motion records were extracted from the Pacific Earthquake Engineering Research Center (PEER) database. These records were scaled in order to cover all damage state levels, leading to 232 ground motion records (from the 171 original records). The

histogram in Figure 13 illustrates the distribution of peak ground acceleration (PGA) across all records, along with the respective response spectra. It is important to understand that the set of selected ground motion records can affect significantly the resulting fragility results (Kohrangi et al. 2017). Therefore, the fragility models proposed in this study should be used with caution in regions with tectonic characteristics distinct from the coast of Peru (e.g. stable continental regions).

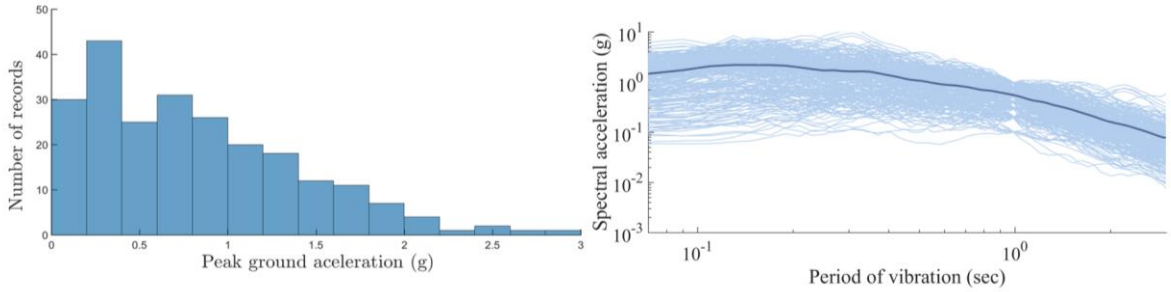

Figure 13. Left: distribution of records according to the PGA. Right: Response spectrum of selected records and mean.

The calculation of the seismic demand imposed by each record was performed following the procedure proposed by Silva *et al.*, (2013). In this process, the demand is initially represented by the 5% damped spectra. Then, at each limit state, the inelastic displacement is calculated by applying a correction factor to the elastic displacement. In the Eurocode 8 (CEN, 2004), the following equation is proposed for the calculation of the correction factor:

$$\eta = \sqrt{\frac{10}{5 + \xi_{eq}}} \tag{7}$$

where ξ_{eq} stands for the equivalent viscous damping at each limit state. Priestley et al. (2007) proposed the following equation for the estimation of this parameter.

$$\xi_{eq} = 0.05 + c/\pi \cdot (\mu - 1)/\mu \tag{8}$$

where c is a constant whose value has been proposed by Naveed *et al.*, (2010) as 0.27. This value was obtained through nonlinear regression of experimental results of masonry piers. μ is the ductility for a given limit state defined as the ratio between the displacement at the associated limit state, and the displacement at the yielding point.

DERIVATION OF FRAGILITY FUNCTIONS

The allocation of each model into a damage state given a specific ground motion record is performed following the Displacement-based Earthquake Loss Assessment (DBELA) theory.

In this method, the displacement capacity and demand at each limit state (see Table 4 and Table 5) is compared; if the demand exceeds the capacity, the next limit states is checked successively, until the demand no longer exceeds the capacity and a damage state can be defined. If the demand also exceeds the capacity of the last limit state, the building is assumed to have collapsed. This process is repeated for all the buildings, allowing the calculation of a Probability Damage Matrix (PDM). This matrix represents the percentage of models in each damage state per ground motion record.

A second process is performed to investigate the most efficient intensity measure to define the fragility functions. In this process, a correlation factor (R^2) is computed between the cumulative percentage of buildings in each damage state and the probabilities provided by the lognormal distribution. The results of this process are shown in Figure 14. The highest correlation coefficient is used to identify which period of vibration should be used for the definition of the fragility curves. The best correlation for 1-story formal and informal buildings was found for a period of vibration close to the PGA, while for 2-story formal and informal buildings 0.20 sec led to a higher correlation.

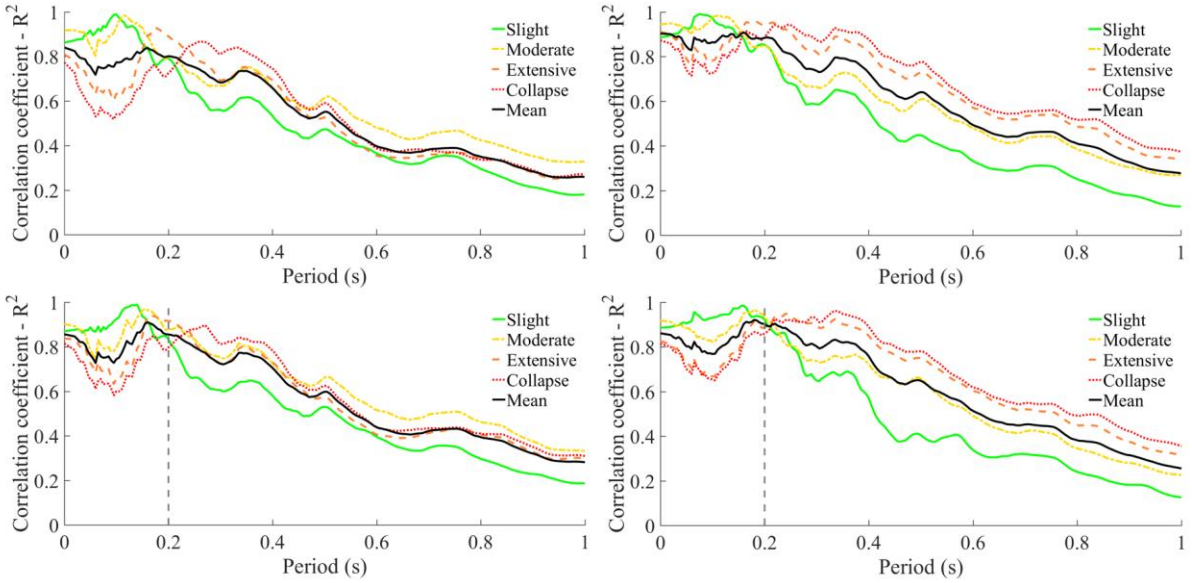

Figure 14. Correlation coefficient for each damage state along the periods for 1-story formal building (a), 1-story informal building (b), 2-story formal buildings (c) and 2-story informal building (d). Black line shows the mean of the correlation coefficients of all the damage states.

Using the most efficient intensity measure assessed previously and the maximum likelihood method, four fragility curves per building class were derived, as presented in Figure 15. The associated statistical parameters are described in Table 8.

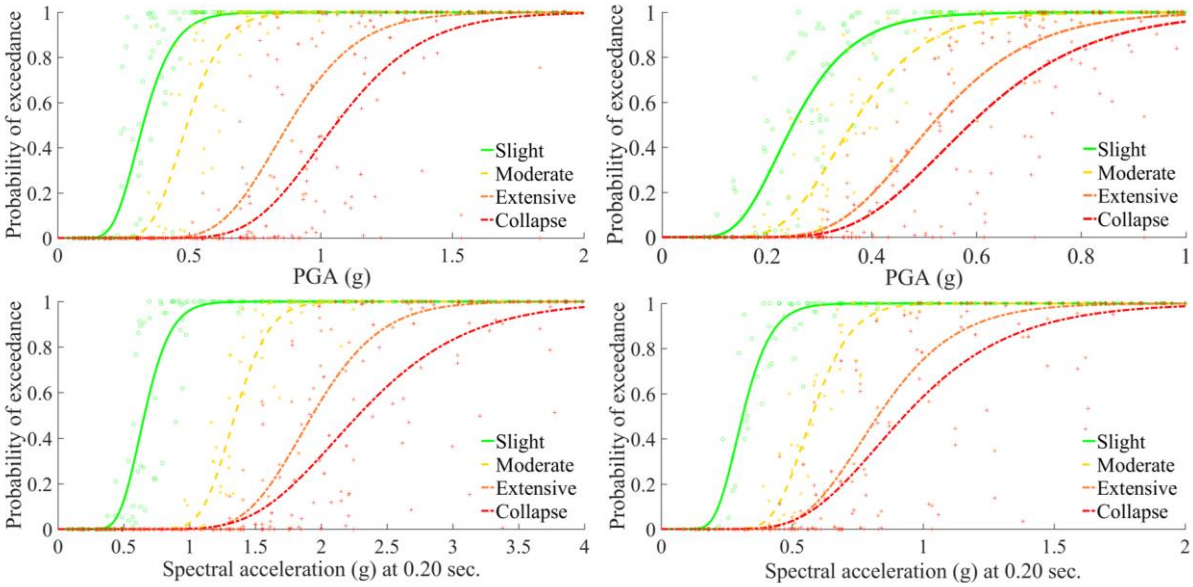

Figure 15. Fragility curves for formal and informal CM buildings of 1-story (a) and (b), respectively. Fragility curves for formal and informal CM buildings of 2-story (c) and (d), respectively.

Table 8. Damage threshold associated to Damage States.

Typology	Parameter	Damage State			
		Slight	Moderate	Extensive	Collapse
1-story formal buildings (PGA)	Mean	0.338	0.503	0.901	1.086
	Std. deviation	0.010	0.013	0.047	0.073
1-story informal buildings (PGA)	Mean	0.266	0.379	0.537	0.615
	Std. deviation	0.010	0.013	0.025	0.037
2-story formal buildings (Sa at 0.20 sec.)	Mean	0.679	1.280	1.847	2.283
	Std. deviation	0.052	0.132	0.199	0.605
2-story informal buildings (Sa at 0.20 sec.)	Mean	0.305	0.563	0.893	0.992
	Std. deviation	0.006	0.021	0.080	0.107

ESTIMATION OF SEISMIC RISK METRICS

In this section, the previously presented sets of fragility functions are combined with the recently released probabilistic seismic hazard model for South America (https://sara.openquake.org/) to calculate two risk metrics: average annual collapse probabilities and average annual loss ratios. This hazard model characterizes active seismic sources in South America in terms of geometry, magnitude-frequency distribution, occurrence rates and range of possible maximum magnitudes. Four tectonic regimes were considered: subduction interface, subduction intraslab, active shallow crust and stable shallow crust. The seismicity of the shallow areas was modelled using a combination of

distributed seismicity (area sources for both active shallow crust and stable continental regions) and crustal fault sources. The subduction interface seismicity was modelled as large fault sources, while the subduction in-slab seismicity was modelled as 3D volumes of ruptures. The epistemic uncertainty coming from the selection of ground motion prediction equations (GMPEs) for each tectonic region was considered using a logic tree. Additional information about this model, including the selection of the GMPEs, can be found in Garcia et al. (2017).

These calculations were performed using the OpenQuake-engine (Silva et al. 2014c, Pagani et al. 2014), an open-source software for seismic hazard and risk analysis. The steps for the calculation of the two risk metrics are presented below:

1. For the city of Lima, a mean seismic hazard curve (rate of exceeding a given ground shaking intensity measure - λ_{IM}) is calculated considering the intensity measures presented in Figure 15, and a time span of one year. These calculations were performed assuming two types of soil conditions: soil (VS_{30} = 360 m/s) and rock (VS_{30} = 760 m/s).

2. For the calculation of the average annual collapse probability, the seismic hazard curve is convoluted with the collapse fragility curve ($P(C|im)$), leading to a curve describing the collapse rate for different return periods. This curve is then mathematically integrated to obtain the average annual collapse rate (λ_c), as described by the equation below. For a time span of one year, this annual rate can be approximated to an annual probability.

$$\lambda_c = \int P(C|im).|d\lambda_{IM}(im)| \tag{9}$$

3. For the calculation of the average annual loss ratio, each set of fragility function is converted into a vulnerability function, by assuming a damage ratio for each damage state. The damage ratios proposed by Yepes-Estrada and Silva (2017) for South America were used for this purpose (slight 0.05, moderate 0.20, extensive, 0.6 and collapse 1.0). Then, each vulnerability function is convoluted with a seismic hazard curve (per location), leading to a loss ratio exceedance curve. Similarly to step 2, this curve can be mathematically integrated to calculate the average annual loss ratio (λ_{LR}), as expressed by the following equation:

$$\lambda_{LR} = \int_0^{\infty} LR(im).|d\lambda_{IM}(im)| \tag{10}$$

The resulting average annual collapse probability and loss ratio are presented in Figure 16 and 17, respectively.

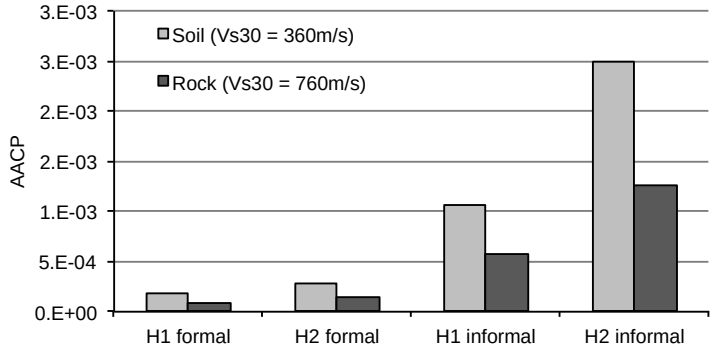

Figure 16. Average annual collapse probability for the four building typologies.

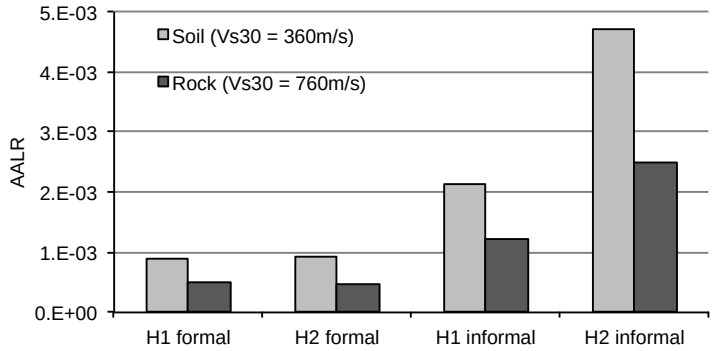

Figure 17. Average annual loss ratio for the four building typologies.

The results regarding the average annual collapse probabilities indicate that informal construction has a probability of collapse 2 and 5 times higher than formal construction for 1 and 2 storeys, respectively. It is also relevant to note that the annual probabilities of collapse for the formal construction are below common acceptable risk thresholds in regions with moderate to high seismic hazard (e.g. California $2x10^{-4}$, New Zealand $1x10^{-4}$), but well above the safety levels supported by countries with lower seismicity (e.g. Switzerland, United Kingdom $1x10^{-5}$) (Silva *et al*. 2015). The average annual loss ratios are relatively high (e.g. Yepes-Estrada *et al.*, 2017) for both the informal and formal construction, which signifies that although the structural safety might be satisfied, lower levels of damage might still cause significant losses.

CONCLUSIONS

Fragility curves have been derived for confined masonry buildings in the metropolitan area of Lima – Peru, formally or informally constructed. A mechanics-based procedure was

followed for the computation of simplified capacity curves, based on the approach proposed by Borzi et al. (2008), Restrepo-Velez (2004) and Benedetti and Petrini (1984). The definition of the drift capacity of the structures was defined using experimental results reported by Salinas and Lázares (2007), Araoz and Velezmoro (2012) and Manchego et al. (2016). The availability of experimental data was fundamental in this study in order to properly characterize the structural capacity of the confined masonry walls. Previous studies (e.g. Villar et al. 2017) have focused mostly on numerical modelling and expert judgement, which may lead to biased results. Similar campaigns should be supported to investigate other features in confined masonry (e.g. effect of adjacent buildings, structural irregularities, etc), and be extended to other building classes.

This process was complemented with information from surveys of existing buildings, which improved the reliability and representativeness of this study. The seismic demand was represented by a large set of ground motion records selected considering the tectonic environment around the city of Lima. This allowed propagating the record-to-record variability. The resulting fragility functions can be used for seismic risk assessment or estimation of damage and losses from specific scenarios. In general, the results from this study are more conservative than what was obtained by Villar et al. (2007). However, since this study is specifically focused in CM buildings of Lima, considerable differences were expected.

Considering the seismic hazard at the city of Lima, two risk metrics were calculated for the four building classes. These results indicated that the seismic safety of the informally built structures is not complaint with the safety levels accepted in regions with similar seismic hazard. Moreover, according to the Peruvian Seismic Code, a spectral acceleration of 1.125g (0.45g times 2.5 amplification factor) can be expected in coastal areas such as Lima. With this seismic input, 1 and 2-story informal CM buildings may expect to suffer around 4% and 51% of collapses, respectively, while their formal counterparts present negligible probabilities of collapse. Such finding is a clear demonstration of the value in endorsing seismic provisions during the design and construction stage, and an encouragement to the improvement of the seismic performance of existing structures through seismic retrofitting.

ACKNOWLEDGEMENTS

The authors wish to express their gratitude to the Pontifical Catholic University of Peru (PUCP), to the National Council of Science, Technology and Technological Innovation

(CONCYTEC) in the framework of the 027-2015-FONDECYT agreement, and to the Global Earthquake Model (GEM). To all these institutions for the financial aid, without this work could not have achieved. Also, the authors appreciate the support and guidance of Dr. Marcial Blondet, who provided the results of the buildings' surveys.

REFERENCES

Alcocer, S., Guillermo, J., Vazquez, A., 2004. Response Assessment of Mexican Confined Masonry Structures Through Shaking Table Tests, Paper No. 2130, in *Proceedings, 13th World Conference on Earthquake Engineering*, 01–60 August, 2004, Vancouver, Canada.

Araoz, T., Velezmoro, J., 2012. Reforzamiento de viviendas existentes construidas con muros confinados hechos con ladrillos pandereta (In Spanish). M.Sc. Thesis, Pontifical Catholic University of Peru, Peru.

Benedetti, D., Petrini, V., 1984. Sulla vulnerabilità sismica di edifici in muratura: Proposta su un metodo di valutazione. *L'industria delle Costruzioni (In Italian)* **149**, 66–74.

Blondet, M., Dueñas, M., Loaiza, C., Flores, R., 2004. Seismic Vulnerabilidad of informal Construccion Dwellings in Lima, Peru: Preliminary Diagnosis, Paper No. 2122, in *Proceedings, 13th World Conference on Earthquake Engineering*, 01–06 August, 2004, Vancouver, Canada.

Blondet, M., Tarque, N. and Velásquez, J.,2006. Seismic risk assessment of informally built confined masonry dwellings in Peru. Paper No. 627, *In Proceedings, 1st European Conference on Earthquake Engineering and Seismology*. 03-08 September, 2006, Geneva, Switzerland.

Borzi, B., Crowley, H., Pinho, R., 2008. Simplified Pushover-Based Earthquake Loss Assessment (SP-BELA) Method for Masonry Buildings, *Int. Journal of Arch. Heritage* **2 (4)**, 353–376.

Calvi, G., 1999. A displacement-based approach for vulnerability evaluation of classes of buildings, *Journal of Earthquake Engineering* **3 (3)**, 411–438.

Centro Nacional de Prevención de Desastres (CENAPRED), 2001. *Estudio analítico de estructuras de mampostería confinada, Tech. Rep. CENAPRED*, Mexico, D.F.

Douglas J, Edwards B. (2016). Recent and future developments in earthquake ground motion estimation. *Earth-Science Reviews* **160**, 203-219.

Doherty, K., Griffith, M., Wilson, J., 2002. Displacement-based seismic analysis for out-of-plane bending of unreinforced masonry walls, *Earth. Eng. Structural Dynamics* **31**, 833–850.

Earthquake Engineering Research Institute (EERI), 2007. *The Pisco, Peru, Earthquake of August 15, 2007, Tech. Rep. EERRI Special Earthquake Report.* Oakland, Califormia.

Earthquake Engineering Research Institute (EERI), 1996. *The February 21, 1996 Chimbote Tsunamis in Peru, Tech. Rep. EERRI Special Earthquake Report.* Oakland, Califormia.

Federal Emergency Management Agency (FEMA), 2007. *Interim Testing Protocols for Determinating the Seismic Performance Characteristics of Structural and Nonstructural Components, Report No. FEMA-461,* Washington, DC.

García, H., Degrande, G., 2017. Performance and Seismic Vulnerability of a Typical Confined Masonry House Used in Cuenca Ecuador. Paper No. 4562, in *Proceedings, 16th World Conference on Earthquake Engineering*, 09–13 January, 2017, Santiago, Chile.

Global Earthquake Model (GEM), 2015. South American Risk Assessment (SARA) Project, available at https://sara.openquake.org/ (last accessed 1 September 2017).

Lagomarsino, S., Giovinazzi, S., 2006. Macroseismic and Mechanical Models for the Vulnerability and Damage Assessment of Current Buildings. *Bull. of Earth. Eng.* **14 (S1)**, 1–37.

Loaiza, C., Blondet, M., 2002a. Confined Masonry Building. World Housing Encyclopedia Technical Report. http://www.world-housing.net/WHEReports/wh100021.pdf.

Loaiza, C., Blondet, M., 2002b. Confined Masonry Houses. World Housing Encyclopedia Technical Report. http://www.world-housing.net/WHEReports/wh100012.pdf.

Kohrangi M, Bazzurro P, Vamvatsikos D, Spillatura A. (2017) Conditional spectrum-based ground motion record selection using average spectral acceleration. Earthquake Engineering & Structural Dynamics 46:10, 1667-1685.

MATLAB R2015a, The MathWorks, Inc., Natick, Massachusetts, United States.

Manchego, A., Pari, R., Tarque, N., Blondet, M., 2016. Respuesta experimental de muros de albañilería confinada para cargas cíclicas en el plano en Lima. Paper No.OS-6-18, in *Proceedings, 1th World Eng. Conference on Disaster Rik Reduction*, 05-06 December, 2016, Lima, Peru.

Monroy, M., Bolaños, A., 2004. Espectros de Peligro Sísmico Uniforme para el Perú (In Spanish). M.Sc. Thesis, Pontifical Catholic University of Peru, Peru.

MVCS. Norma Técnica Peruana E.070 Albañilería (In Spanish). Ministerial Resolution N°011-2006-Vivienda. Ministerio de Construcción y Vivienda, Lima, Perú. 2006

Naveed, A., Crowley, H., Pinho, R., Qaisar, A., 2007. Displacement-Based Earthquake Loss Assessment of Masonry Buildings in Mansehra City – Pakistan. *Journal of Eathquake Engineering* **14 (S1)**, 1–37.

Priestley, M., Calvi, G., Kowalsky, M., 2007. *Masonry Structures, in Displacement-Based Seismic Design of Structures*. 1st edition, IUSS Press, Pavia, Italy, 413-454.

Restrepo-Velez, L., 2004. A simplified mechanics-based procedure for the seismic risk assessment of unreinforced masonry buildings, Paper No. 2561, in *Proceedings, 13th World Conference on Earthquake Engineering*, 01–06 August, 2004, Vancouver, Canada.

Riahi, Z., Elwood, K., Alcocer, S., 2009. Backbone Model for Confined Masonry Walls for Performance-Based Seismic Design, *Journal of Structural Engineering* **135 (6)**, 644–654.

Rodriguez, M., Blondet, M., 2004. Evaluation of Housing Losses in Recent Earthquakes in Latin America, Paper No. 2103, in *Proceedings, 13th World Conference on Earthquake Engineering*, 01–06 August, 2004, Vancouver, Canada.

Salinas, R., Lázares, F., 2008. Seismic Performance of Confined Masonry Buildings with Tubular Bricks in Developing Areas, in *Proceedings, 14th World Conference on Earthquake Engineering*, 12–17 October, 2008, Beijing, China.

San Bartolomé, 1994. *Construcciones de Albañilería (In Spanish)*. 1st edition, Pontificia Universidad Católica Editorial Fund, Lima, Peru, 127-170.

Silva, V., Varum. H., Crowley, H., Pinho, R., 2013. Extending Displacement-Based Earthquake Loss Assessment (DBELA) for the Computation of Fragility Curves, *Eng. Structures* **56**, 343–356.

Silva, V., Crowley, H., Pinho, R., Varum, H. (2014a) "Investigation of the Characteristics of Portuguese Regular Moment-frame RC Buildings and Development of a Vulnerability Model". Bulletin of Earthquake Engineering, 13(5):1455-1490.

Silva, V., Crowley, H., Pinho, R., Varum, H. and Sousa, R. (2014b) "Evaluation of analytical methodologies to derive vulnerability functions". Earthquake Engineering and Structural Dynamics, 43(2):181-204.

Silva, V., Crowley, H., Pagani. M., Monelli. D., Pinho, R. (2014c). Development of the OpenQuake-engine, the Global Earthquake Model's open-source software for seismic risk assessment. *Natural Hazards* **72(3)**, 1409–1427.

Silva V, Crowley H, Bazzurro P (2015) "Exploring Risk-targeted Hazard Maps for Europe". Earthquake Spectra.

Seismicity and Seismic Risk in the Andean Region. (In Spanish) Sismicidad y Riesgo Sísmico en la Región Andina. (1985) *Earthquake catalogue for South America*. Lima, Peru.

Tomaževič, M., Gams, M., 1997. Verification of Seismic Resistance of Confined Masonry Buildings, *Earthquake Engineering and Structural Dynamics* **26**, 1076–1088.

Tavera, H., Buforn, E., 2001. Source mechanism of earthquakes in Peru. *J. of Seismo*. **5(4),** 519-540

Themelis, S., 2008. Pushover Analysis for Seismic Assessment and Design of Structures. Ph. D. Thesis, Heriot-Watt University, United Kingdom.

Tarque N., Mosqueira M., 2005. Recomendaciones Técnicas para Mejorar la Seguridad Sísmica de Viviendas de Albañilería Confinada de la Costa Peruana (In Spanish). M.Sc. Thesis, Pontifical Catholic University of Peru, Peru.

Tomaževič, M., Gams, M., 2012. Shaking table study and modelling of seismic behavior of confined AACC masonry buildings, *Bulletin of Earthquake Engineering* **10**, 863–893.

Tomaževič, M., Gams, M., 1997. Verification of Seismic Resistance of Confined Masonry Buildings, *Earthquake Engineering and Structural Dynamics* **26**, 1076–1088.

United Nations, 2013. *Global Assessment Report on Disaster Risk Reduction*, *Report 2013*, New York, United States.

Varela-Rivera, J., Navarrete-Macias, D., Fernandez-Baqueiro, L., Moreno, E., 2011. Out-of-plane behavior of confined masonry walls, *Eng. Structures* **33**, 1734–1741.

Worden, B., Wald, D., 2016. ShakeMap Manual. USGS Technical Report. http://dx.doi.org/10.5066/F7D21VPQ.

Yañez, F., Astroza, M., Holmerg, A., Ogaz, O., 2004. Behavior of Confined Masonry Shear Walls with Large Openings. Paper No. 3438, in *Proceedings*, *13th World Conference on Earthquake Engineering*, 01–06 August, 2004, Vancouver, Canada.

Yepes-Estrada, C., Silva, V., Valcarcel, J., Acevedo, A., Tarque, N., Hube, M., Coronel, G., Santa María, H., 2017. Modeling the Residential Building Inventory in South America for Seismic Risk Assessment, *Earthquake Spectra* **33(1)**, 1–24.

Yepes-Estrada, C., Silva V., 2017. Probabilistic seismic risk assessment of the residential building stock in South America. Paper No. 2050, in *Proceedings, 16th World Conference on Earthquake Engineering*, 09–13 January, 2017, Santiago, Chile.